HREM study of the matrix-pirecipitate interface structure and deformation mechanisms in a cobalt based superalloy

J.-M. Penisson

Classification
Physics Abstracts
61.70

HREM study of the matrix-precipitate interface structure and deformation mechanisms in a cobalt based superalloy

J.-M. Penisson

Département de Recherche Fondamentale, Service de Physique, CENG 85 X, 38041 Grenoble Cedex, France

(*Received June 6, 1990, accepted December 27, 1990*)

Résumé. — La structure d'un superalliage Co-Ni-Cr-Nb a été étudiée par microscopie électronique à haute résolution. Une phase durcissante de structure hexagonale ordonnée est présente après un recuit de vieillissement à des températures comprises entre 700 et 850 °C. La relation d'orientation mutuelle matrice-précipité indique que les plans et directions compactes des deux phases sont parallèles. L'interface est constituée par 3 familles de dislocations coins formant un réseau triangulaire. Le champ de déformation de ces dislocations a été modélisé grâce au formalisme des dislocations de Somigliana. Des échantillons ont été déformés en traction à température ambiante et observés en haute résolution. Les mécanismes par lesquels les précipités sont déformés ont été identifiés ainsi que les dislocations responsables de ces déformations.

Abstract. — The structure of a Co-Ni-Cr-Nb superalloy has been studied using high resolution electron microscopy. An ordered hexagonal phase precipitates during annealing at temperatures from 700 to 850 °C. The compact planes and compact directions of the fcc matrix and precipitates are mutually parallel. The matrix precipitate interface is constituted by 3 sets of edge dislocations in a triangular distribution. The dislocation strain field has been calculated using the formalism of the Somigliana dislocations. Traction experiments were performed at room temperature and deformed samples were observed using HREM. The deformation mechanisms and gliding dislocations have been identified.

1. Introduction.

Superalloys have been developed mainly for their very good mechanical properties. This appellation covers a wide range of different alloys and a possible classification is based on the composition (for a review on superalloys see Ref. [1]). Two main classes are then distinguished : the nickel and cobalt based superalloys according to their main constituant. The mechanical properties are mainly due to the presence within the matrix of a second phase. This second phase is produced by the addition of strengthening elements to the alloy. In Ni based alloys, aluminium is one of the most employed element and leads to the precipitation of Ni_3Al which has an ordered $L1_2$ structure [2]. In Co based alloys, the strengthening in mostly due to the presence of carbides although structural strengthening can also be obtained by addition of Ti or Al [3]. The precipitated phases act as barriers for the motion of dislocations. It is then essential to know the crystallographical structure of these

phases as well as the structure of the matrix-precipitate structure. Because of the accuracy of the atomic position determination, high resolution electron microscopy (HREM) is one of the most powerfull techniques which can be used for these studies. For a special use, a new superalloy has been designed with a composition which is intermediate between Ni and Co superalloys. This particular composition was choosen to give special magnetic properties to the alloy. The strengthening element is niobium and a new ordered hexagonal lamellar phase precipitates during annealing treatments. The composition of the precipitates was investigated by microanalysis and their structure was determined using electron diffraction and HREM associated with image simulations. The matrix-precipitate interface structure was investigated by weak beam dark field and HREM. After deformation at room temperature, some precipitates are sheared by the motion of gliding dislocations. The geometry of the possible slip systems within the matrix and the precipitates have been investigated and the possible Burgers vectors determined.

Although this study represents a particular case, it will be shown that the use of HREM can provide very localised structural informations which are complementary to the ones obtained by other methods.

2. Experimental techniques.

2.1 ALLOY ELABORATION, THERMAL AND MECHANICAL TREATMENTS. — The exact composition in atomic percentage is :

Co 37.6 Ni 36.8 Cr 22.5 Nb 3.1 .

The alloy was elaborated from very pure elements which are cast under vacuum. The ingot is then cold rolled to a thickness 0.5 mm. An homogeneisation treatment for 24 h at 1 200 °C under an argon atmosphere is followed by an annealing at temperatures from 700 to 850 °C for 24 to 196 h. 3 mm discs were then punched and thinned in an electrochemical cell. The precipitates can be extracted from the matrix using the appropriate chemical bath and deposited on a carbon coated grid. This procedure is used for the study of the precipitate structure. The tensile samples are 30 by 5 mm and 0.5 mm thick. They undergo a 2 % deformation at room temperature. Samples for electron microscopy are taken from the central part of them in which the deformation is maximum.

2.2 ELECTRON MICROSCOPY. — HREM experiments were performed on a 4000-EX JEOL microscope working at 400 kV. This microscope is fitted with a low spherical aberration objective pole piece (Cs = 1 mm) which gives a very good resolution [4]. In these conditions, all the low index planes of both matrix and precipitates can be visualised with a high contrast. The chemical composition of the precipitates was investigated using a Philips EM 430 fitted with an EDAX spectrometer.

2.3 IMAGE SIMULATIONS. — In order to determine the best imaging conditions : specimen thickness and defocus, « maps » of contrast were calculated on both matrix and precipitate structures. These calculations were performed using the NCEMSS package developed by Kilaas [5]. Simulated images were also obtained from calculated models of interfacial dislocations and compared to experimental images. In some cases, the experimental images were also processed by Fourier filtering either to reduce the noise or to isolate the contribution of some diffracted beams in order to simplify the contrast analysis.

3. Experimental results.

3.1 ALLOY MORPHOLOGY. — After the homogeneisation treatment at 1 200 °C all the elements form a solid solution. The second phase precipitates only after a 24 h incubation time [6]. The precipitates then appear as thin lamellas whose thickness increases rather slowly with the annealing time. The volume fraction of the precipitates increases linearly, the maximum being around 12 %. Due to the cold work treatment, many grains have ⟨011⟩ orientation which is suitable for HREM experiments. In this particular matrix orientation, 4 orientation variants of the precipitates can be seen : figure 1. The analysis of the traces of the precipitates indicates that they are parallel to the 4 {111} matrix planes.

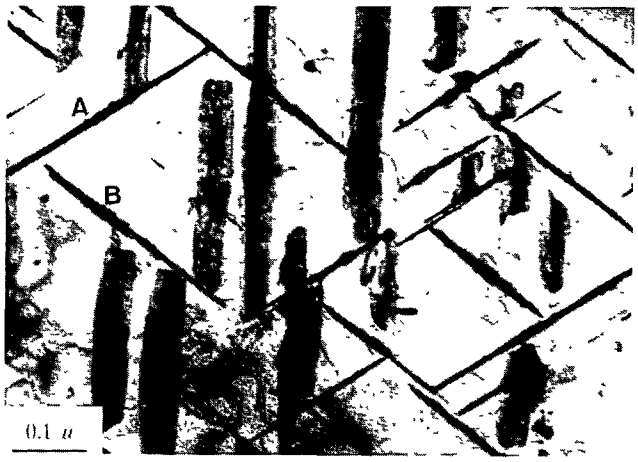

Fig. 1. — Alloy annealed for 72 h at 800 °C. The matrix has a ⟨011⟩ orientation and 4 orientation variants are present. Two variants (A and B) are seen end on, the two others being inclined.

3.2 PRECIPITATE COMPOSITION AND STRUCTURE. — The microanalysis experiment showed that the precipitate composition can written as [7] :

$$(Co_{0.36}Ni_{0.61}Cr_{0.03})_3Nb\ .$$

The electron diffraction patterns clearly revealed a six fold symmetry while HREM images of edge on precipitates showed an ABAB.. stacking sequence (Fig. 2). It should be remarked that this sequence is only visible in very thin areas of the precipitates. When the thickness increases, a super period appears at the same time as the kinematically forbidden 0001 diffraction spot becomes more intense. It has been verified using multislice simulations that the 0001 spot is effectively present due to double diffraction but its intensity is too small to reproduce the experimental images. If a small additional misorientation is added (mainly a beam tilt) then then 0001 intensity increases and the super period appears in agreement with the experimental images so that it is not necessary to invoke a compositional modulation along the c axis. Some precipitates are faulted and a local ABC sequence can be seen. These faults correspond to the I_1 faults in the terminology of Hirth and Lothe [8]. Through focus series were obtained on extracted precipitates which are then oriented with their 6-fold axis parallel to the electron beam. All these results are consistent with a DO_{19} structure with $c/a = 1.62$.

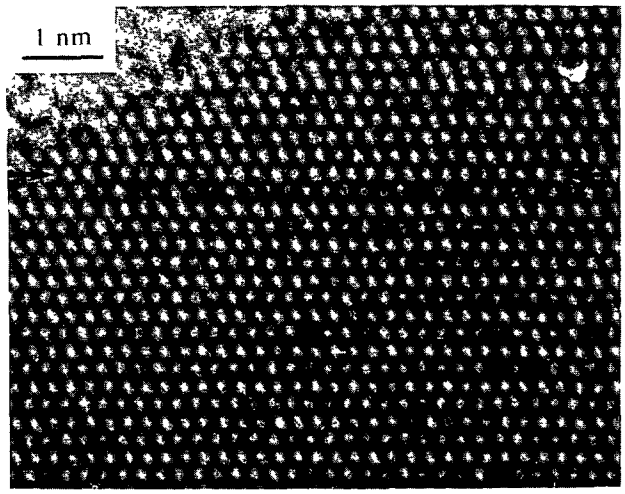

Fig. 2. — 100 kV high resolution image of the precipitate structure in the [11$\bar{2}$0] orientation. The ABAB stacking sequence is visible. An I_1 stacking fault (arrowed) is present represented by the sequence ABABACACA. The specimen is very thin and well oriented so that the forbidden 0001 diffraction spot has a very low intensity : only a very faint contrast modulation parallel to the c axis can be seen.

3.3 INTERFACE STRUCTURE. — Matrix and precipitate have a special orientation relationship in which the compact planes of both phases are strictly parallel and in these planes, the compact directions are also parallel. This relation can be written as :

$$(0001)_p // (111)_m \quad \text{and} \quad \langle 11\bar{2}0 \rangle_p // \langle 110 \rangle_m$$

The interface plane is also parallel to the compact planes. There is a 2 % misfit between the two phases, the precipitate parameter being larger than the matrix one. When a single

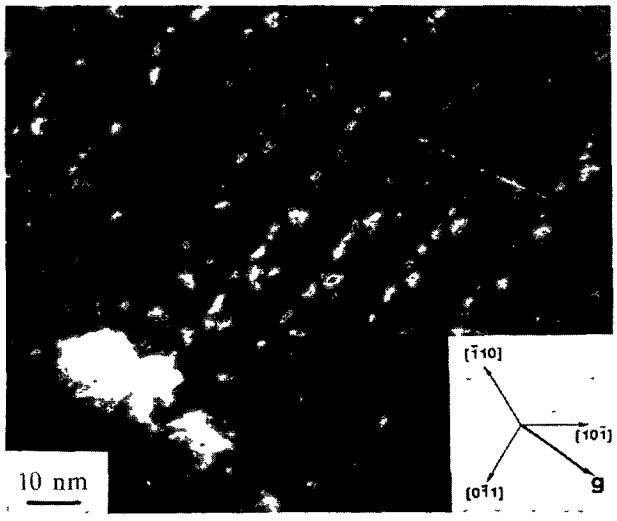

Fig. 3. — Weak beam dark field image of the interface. A 4$\bar{2}\bar{2}$ diffraction vector is used : 3 sets of 1/6 ⟨112⟩ edge dislocations are then visible.

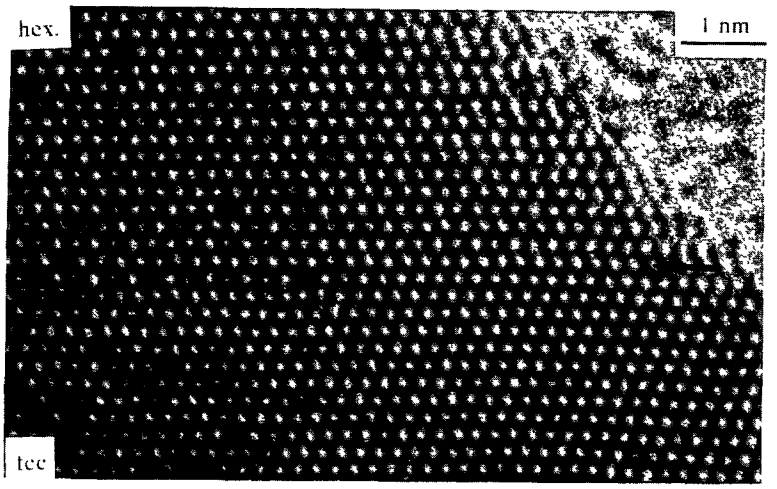

Fig. 4. — High resolution image of the edge on interface. A pure edge interfacial dislocation associated with a biatomic step is present.

interface is observed in an orientation nearly perpendicular to the incident electron beam and using the weak beam technique, it appears as made of 3 sets of edge dislocations which have a triangular distribution : figure 3. The spacing between these dislocations is around 12 nm and their Burgers vector is $b = 1/6 \langle 112 \rangle$. When the interface is observed edge on in HREM (Fig. 4), it can be seen that each dislocation is associated with a 2 d_{111} step. In fact a carefull examination of the images reveals that dislocations with a 30° Burgers vector are also present. This fact will be explained later. It should be remarked that the steps associated with the 90° and 30° dislocations have the same height but an opposite sense.

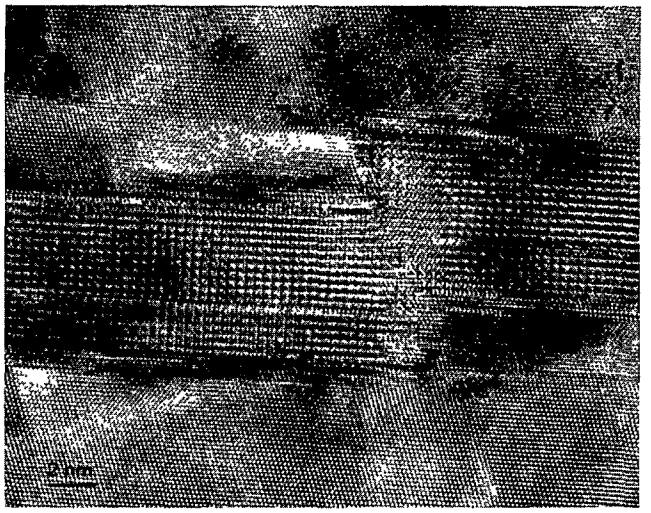

Fig. 5. — High resolution image of a sheared precipitate. Matrix dislocations glide on the 111 plane making a 70.5° with respect to the interface. The glide plane within the precipitate is the $10\bar{1}1$ pyramidal plane. The amount of shear can be measured by the relative displacement of the preexisting stacking fault across the glide plane.

3.4 DEFORMATION. — Samples with different annealing treatments were deformed at room temperature. When the precipitate volume fraction is small, the matrix deforms by twinning. When the precipitation of the DO_{19} phase takes place, the precipitates can be sheared by the motion of gliding dislocations : figure 5. The moving dislocations are 1/2 ⟨110⟩ 60° dislocations. Within the fcc matrix, they are dissociated into 90 and 30° Shockley partials. The shear of the precipitates is identified by the creation of a new interface and also by the shear of the preexisting faults : figure 6. In all the cases no shear smaller than 4 atomic planes have been found. The glide plane in the precipitates can be identified as the first pyramidal plane which makes a 9° angle with the corresponding matrix glide plane. When the shear is large, some additional rotations appear in the matrix near the newly created interface. Up to now, no other deformation mechanisms have been found. In particular, there is no cut of the precipitate by matrix twins as was found by Mahon and Howe in a two phase TiAl alloy which has a similar morphology [9].

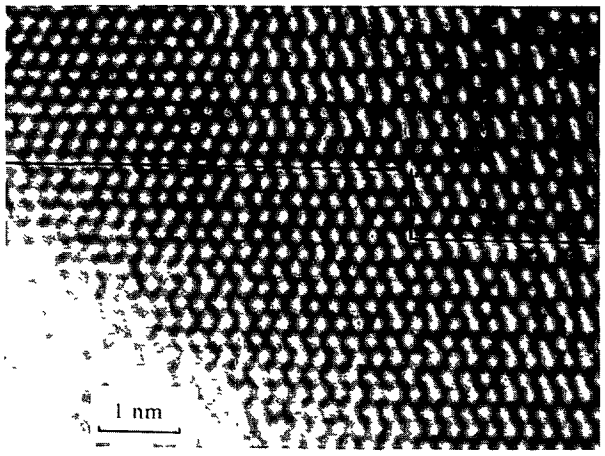

Fig. 6. — Stacking fault sheared by the motion of gliding dislocations. The minimum observed shear corresponds to 4 matrix dislocations.

4. Interpretation of the results.

4.1 STRUCTURE OF THE SECOND PHASE. — The microanalysis showed that cobalt is present within the precipitates and this presence has an influence on their structure. In alloys without Co, the second phase is Ni_3Nb which can be either orthorhombic (β Ni_3Nb) or quadratic depending on the thermal treatment [10]. The coexistence of a 6 fold symmetry axis with the ABAB stacking sequence and an ordered structure leads to the DO_{19} structure. This is an ordered hexagonal structure and as pointed out by Marcinkowski [11], it is very similar to the $L1_2$ structure ; the structure of the compact planes being the same while the stacking is ABC in the $L1_2$ case. The structure is also very similar to the orthorhombic Ni_3Nb the differences being the Nb atom distribution in the compact planes which is triangular for DO_{19} and rectangular in the orthorhombic case. Finally the images of these two different structures have been imaged in HREM and compared to simulated images [7] and the agreement is quite good. It should be remarked that if the second phase was Ni_3Nb, 12 orientation variants would be present. The structure change when cobalt is present in the alloy can be interpreted in terms of conduction electron concentration [7].

When stacking faults are present, they are always intrinsic corresponding to the sequence :

ABABACACA...

These I_1 faults cannot be formed by a simple shear and they have the smallest energy [8]. In fact, the precipitates have an ordered structure and it seems possible to envisage the existence of super (SISF) and complex (CSF) faults in the same way as in the $L1_2$ structure [12]. Image simulations [13] showed that using special experimental conditions (specimen thickness and defocus), the ordered structure can be visible so that SISF and CSF should be distinguished. Some HREM pictures have already been obtained on dissociated screw dislocations in NI_3Al [14].

4.2 INTERFACE STRUCTURE. — The interface plane is parallel to the compact planes of both phases. These planes have the same symmetry and the only difference is the misfit between them. In similar cases, the interface is generally a honeycomb net of edge dislocations with an hexagonal dislocation distribution [15]. The geometry of the observed net can be explained using the same ideas as those developed for the twist boundaries in fcc metals [8]. The main results of this analysis will be published soon [16]. It is based on the possible dissociation of some of the dislocation nodes leading to the observed geometry. The discrepancy between weak beam dark field results : 3 sets of 1/6 ⟨112⟩ edge dislocations and the HREM results : presence of both 90° and 30° dislocations can be explained when the geometry of the HREM specimens is considered. These specimens are very thin : typically 100 Å or less. In these conditions, the thickness is smaller than the dislocation spacing and the inclined dislocation lines can rotate under the action of the surfaces leading to the apparition of the observed 30° dislocations.

The interfacial dislocations are misfit dislocations so that their strain field cannot be calculated using the expressions describing a Volterra dislocation. Volterra dislocations have been used by Howe *et al.* to simulate 90° and 30° 1/6 ⟨112⟩ dislocations in the AlAg system in which the misfit between the two phases can be neglected [17]. Bonnet and Marcon [18] proposed to use the concept of Somigliana dislocations [19] to calculate this strain field and a calculation program has been developed by Bonnet *et al.* [20]. The calculations are done using

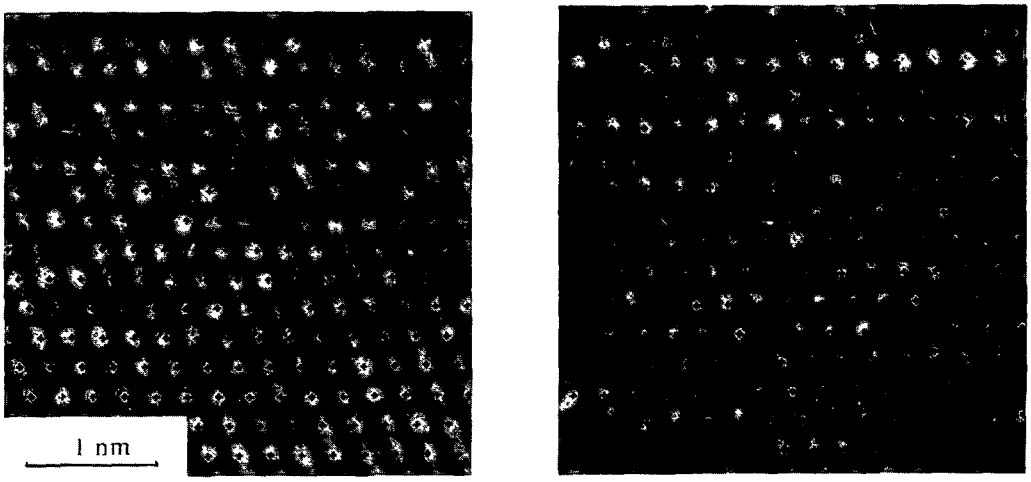

Fig. 7. — Superposition to the HR image (white atomic positions) of the calculated positions around the interfacial dislocations using the Somigliana dislocation concept. a) 90° dislocation ; b) 30° dislocation.

the anisotropic elasticity and as the elastic constant of the DO_{19} phase are unknown, they were replaced by those of Ni_3Nb. A superposition of the calculated positions to the white spots of the high resolution image is shown in figure 7a in the case of the 90° and in figure 7b in the case of the 30° dislocation. Apart from the core itself where the elastic theory cannot be applied, there is a good fit between calculated and experimental atomic positions.

4.3 DEFORMATION MECHANISMS. — When the alloy is deformed at room temperature, both the fcc matrix and the second phase undergo the deformation and one of the problem is to understand the transmission mechanisms of the strains from the matrix to the precipitates. A brief description of these mechanisms has already been published [21].

It must be kept in mind that several different limitations on the observation of the deformation process are present due to the geometry of the specimens and to the observation method. The specimens are polycrystalline and the deformation is not homogeneous. The activated slip systems must be such that they induce a deformation which will be visible on the images. For example, if a precipitate undergoes a shear in a direction parallel to the incident beam it will not be detected. The description is then partial. We will consider only the orientation $(011)_m$ $(11\bar{2}0)_p$ which is suitable for HREM and in this orientation, the propagation of $1/2\ \langle 101\rangle$ or $1/2\ \langle \bar{1}10\rangle$ Burgers vectors on the $1\bar{1}1$ gliding plane.

In the matrix, many dislocations, stacking faults and twins are present. The presence of cobalt lowers considerably the stacking fault energy so that there is a large dispersion in the dissociation length and no stacking fault energy can be measured from the images. These faults are frequently intersected by dislocations or other faults so that they do not seem to represent a strong obstacle to the motion of gliding dislocations. A much stronger obstacle is represented by the twins on which many dislocations are stopped.

When the volume fraction is sufficient, the precipitates participate in the deformation process. The only glide plane which has been observed in the precipitates is the first pyramidal plane $(10\bar{1}1)$. In hexagonal metals, this plane can be observed although it is not the main slip system [22]. The deformation of DO_{19} compounds has also been studied by several authors [23-25]. Ti_3Al is the most studied material and dislocations with Burgers vectors **a**, **c**, **a** + **c** were evidenced by weak beam dark field. The glide planes were the prismatic and the pyramidal planes. In this alloy, the pyramidal plane has a direction in common with the matrix glide plane and it makes the smallest angle with it. The atomic structure of this plane is corrugated. This corrugation is clearly observed in the images of very thin precipitates. A slip on the pyramidal plane involves dislocations with Burgers vectors either **a** or **a** + **c** (these vectors represent perfect dislocations of the hexagonal structure but they are super partials of the DO_{19} ordered structure). If the precipitates are sheared by the motion of dislocations with Burgers vectors **a**, the only possibility is the vector parallel to the incident electron beam so that the resulting shear is invisible using the orientation $\langle 011\rangle_m$ $\langle 11\bar{2}0\rangle_p$. The shear being visible, only **a** + **c** dislocations can be involved. This Burgers vector is rather large and several dissociation reactions are possible :

$$1/3[11\bar{2}3] \rightarrow [0001] + 1/3[11\bar{2}0]$$

$$1/3[11\bar{2}3] \rightarrow 1/6[20\bar{2}3] + 1/6[02\bar{2}3]$$

$$1/3[11\bar{2}3] \rightarrow 1/9[\bar{1}013] + 1/18[2\bar{6}43] + 1/6[\bar{2}023]\,.$$

The first reaction corresponds to $\mathbf{a} + \mathbf{c} \rightarrow \mathbf{a} + \mathbf{c}$. This reaction cannot be considered here because both partials are sessile for the pyramidal slip. The second is the decomposition into

two partials which are in general described as sessile [8]. In the pyramidal slip system, however, they are glissile. Furthermore, the modulus of their Burgers vector corresponds to that of a 60° matrix dislocation gliding on the $(1\bar{1}1)$ plane. It must be remarked here that due to the atomic structure of the pyramidal plane, these Burgers vectors do not lie exactly in the slip plane. Only one Burgers vector is parallel to that of the incoming matrix dislocations so that a small residue is left at the interface. The rearrangement of the internal strains provokes a small rotation of the matrix planes in this region. Up to now, the exact interaction between the residues and the interfacial dislocations has not been studied in detail and further work in needed in this direction.

The precipitate has an ordered structure and the sum of the 2 partials corresponds to a super partial associated to an antiphase boundary (APB). The perfect structure will be recovered if 4 partials glide across the precipitate. This explains why the minimum observed shear is 4 atomic planes (Fig. 6). Shears smaller than this value were observed but in this case, a dislocation and an APB were present.

The third reaction is a complex one proposed by Jones and Hutchinson [26] on the basis of a hard sphere model. Although this possibility could not be formerly discarded, its occurrence in the deformation mechanism seems to be unlikely.

5. Summary and conclusion.

In this study it has been shown how HREM can be used to determine the structure of a new phase and to elucidate some deformation mechanisms. The particular alloy has been elaborated for a special use in accelerometry and its composition reflects this constraint. The second phase which is mainly responsible for the mechanical properties has a structure slightly different from that of β Ni_3Nb, but HREM is sufficiently sensitive to structural details to make a difference between them. This ordered hexagonal structure has several consequences. The firts one is the existence of a rather unusual distribution of the matrix-precipitate interfacial dislocations. This distribution is triangular instead of hexagonal and only the calculation of the energies of the different possible configurations will explain the observed structure. The second consequence of the ordered hexagonal phase is on the deformation mechanisms. The crystallography of the matrix-second phase system increases the occurrence of gliding on the pyramidal plane. Previous calculations show that the Schmid factor for this glide system is of the same order as its counterpart in the matrix. In conclusion, the use of HREM in such studies is able to provide localised information at atomic scale which are complementary of other method like weak beam dark field and diffraction.

Acknowledgments.

G. Regheere is gratefully acknowledged for his contribution to the HREM work and many fruitfull discussions. The author would also acknowledge M. Loubradou and R. Bonnet for the calculation of the atomic positions of the interfacial dislocations.

References

[1] DONACHIE M. J., Superalloy Source Book ASM (1988).
[2] SABOL G. P. and STICKER R., *Phys. Stat. Sol.* **35** (1969) 11.
[3] ROGISTER C., COUTSOURADIS D. and HABRAKEN L., Cobalt (1967) 34.
[4] BOURRET A. and PENISSON J.-M., Jeol News 25E (1987) 1.

[5] KILAAS R., 45th Ann. Proc. EMSA Baltimore (1987) 66.
[6] REGHEERE G., Thèse Université de Grenoble (1989).
[7] REGHEERE G. and PENISSON J.-M., *Scripta Met.* **24** (1990) 301.
[8] HIRTH J. P. and LOTHE J., Theory of dislocations (Mac Graw Hill) 1965.
[9] MAHON G. J. and HOWE J. M., to be published in *J. Phys. France.*
[10] ROYER P., Thèse Université de Nancy (1970).
[11] MARCINKOWSKI M. J., Electron Microscopy and Strength of Crystals G. Thomas and J. Washburn Eds. Interscience Publishers 333 (1963).
[12] KEAR B. H., OBLAK J. M. and GIAMEY A. F., *Met. Trans.* **1** (1970) 2477.
[13] MILLS M. J., *Scripta Met.* **23** (1989) 2061.
[14] CRIMP M. A., *Phil. Mag. Lett.* **60** (1989) 45.
[15] LASALMONIE A. and STRUDEL J. L., *Philos. Mag.* **32** (1975) 937.
[16] REGHEERE G. and PENISSON J.-M., to be published in *J. Phys. France.*
[17] HOWE J. M., DAHMEN U. and GRONSKY R., *Philos. Mag.* **A 56** (1987) 31.
[18] BONNET R. and MARCON G., *Philos. Mag.* **A 51** (1985) 429.
[19] SOMIGLIANA C., *Atti. Acad. naz. Lincei Rc.* **23** (1914) 463, Ibid. **24** (1915) 655.
[20] BONNET R., LOUBRADOU M., CATANA A. and STADELMAN P., to be published, in *Met. Trans.*
[21] PENISSON J.-M. and REGHEERE G. J., *Microsc. Spectrosc. Electron.* **14** (1989) 335.
[22] ADDA Y., DUPOUY J.-M., PHILIBERT J. and QUERE Y., Eléments de Métallurgie Physique, Comm. Energ. Atom. Ed. (1979).
[23] THOMAS M., VASSEL A. and VEYSSIERE P., *Scripta Met.* **21** (1987) 501.
[24] THOMAS M. and VASSEL A., *Philos. Mag.* **A 59** (1989) 1013.
[25] COURT S. A., LOFVANDER J. P. A., LORETTO M. H. and FRASER H. L., *Philos. Mag.* **A 59** (1989) 379.
[26] JONES I. P. and HUTCHINSON W. B., *Acta Met.* **29** (1981) 951.